ChemPubSoc Europe

DOI: 10.1002/cphc.201700815

CHEMPHYSCHEM Articles

VIP *Very Important Paper*

Special Issue

Gold Nanoparticles on Polymer-Wrapped Carbon Nanotubes: An Efficient and Selective Catalyst for the Electroreduction of CO_2

Huei-Ru "Molly" Jhong,[a, b] Claire E. Tornow,[a] Chaerin Kim,[b, c] Sumit Verma,[a, b] Justin L. Oberst,[a] Paul S. Anderson,[a] Andrew A. Gewirth,[a, b] Tsuyohiko Fujigaya,*[b, c] Naotoshi Nakashima,*[b, c] and Paul J. A. Kenis*[a, b]

Multiple approaches will be needed to reduce the atmospheric CO_2 levels, which have been linked to the undesirable effects of global climate change. The electroreduction of CO_2 driven by renewable energy is one approach to reduce CO_2 emissions while producing chemical building blocks, but current electrocatalysts exhibit low activity and selectivity. Here, we report the structural and electrochemical characterization of a promising catalyst for the electroreduction of CO_2 to CO: Au nanoparticles supported on polymer-wrapped multiwall carbon nanotubes. This catalyst exhibits high selectivity for CO over H_2: 80–92% CO, as well as high activity: partial current density for CO as high as 160 mA cm^{-2}. The observed high activity, originating from a high electrochemically active surface area (23 m^2 g^{-1} Au), in combination with the low loading (0.17 mg cm^{-2}) of the highly dispersed Au nanoparticles underscores the promise of this catalyst for efficient electroreduction of CO_2.

1. Introduction

The continuous, steady increase in atmospheric CO_2 levels has been linked to climate change, leading to, for example, erratic weather patterns and rising ocean temperatures.[1] Slowing down or ideally curbing the rise in atmospheric CO_2 levels will require concurrent implementation of multiple approaches, including switching from fossil-fuel-burning power plants to renewable energy sources; increasing the energy efficiency of buildings; increasing the fuel efficiency of vehicles or switching to electric vehicles; and carbon capture and sequestration.[2] Also, addressing the main challenge of implementing renewable sources such as wind and solar, their intermittency will require development of a scalable and broadly deployable means for storage of electricity.

One option to both reduce CO_2 emissions and to provide a potential means for energy storage is the electroreduction of CO_2 to chemicals that can be stored and transported at scale and used upon demand.[3] Technically, electroreduction of CO_2 is analogous to running a fuel cell in reverse. The CO_2 reduction reaction takes place at the cathode, while typically the water oxidation reaction (or an alternative reaction like chlorine evolution) takes place at the anode. Over the past few decades, research has mostly focused on the half-reaction of the cathode (i.e., the CO_2 reduction reaction). Prior work by Hori et al. has shown that the use of different metal catalysts leads to different products.[4] For example, group 1 metals such as Au and Ag lead to carbon monoxide (CO), group 2 metals such as Pb and Sn lead predominantly to formic acid, group 3 metals such as Pt and Fe lead to H_2, while group 4 metals such as Cu lead to mixtures of short hydrocarbons. Here we focus on catalysts for the selective production of CO because CO is a key building block for chemical synthesis, for example through the Fischer–Tropsch process which can produce various hydrocarbons.[5] To date, some of the best performance for the electroreduction of CO_2 to CO has been achieved with precious metal catalysts such as silver (Ag) or gold (Au).[3a,6] Previously, we have reported that under ambient conditions, when using IrO_2 as the anode catalyst in alkaline media (1 M KOH as the electrolyte), a partial current density for CO as high as 250 mA cm^{-2} can be achieved in combination with a Faradaic efficiency for CO of 95%, at energy efficiencies as high as 43% using a gas diffusion electrode (GDE) covered with a catalyst layer of Ag nanoparticles.[7] Furthermore, we have shown that

[a] Dr. H.-R. ". Jhong, Dr. C. E. Tornow, S. Verma, Dr. J. L. Oberst, P. S. Anderson, Prof. Dr. A. A. Gewirth, Prof. Dr. P. J. A. Kenis
Department of Chemistry and Chemical & Biomolecular Engineering
University of Illinois at Urbana Champaign
600 South Mathews Avenue
Urbana, IL 61801 (USA)
E-mail: kenis@illinois.edu

[b] Dr. H.-R. ". Jhong, Dr. C. Kim, S. Verma, Prof. Dr. A. A. Gewirth, Prof. Dr. T. Fujigaya, Prof. Dr. N. Nakashima, Prof. Dr. P. J. A. Kenis
International Institute for Carbon Neutral Energy Research (WPI-I2CNER)
Kyushu University, 744 Moto-oka
Nishi-ku, Fukuoka 819-0395 (Japan)

[c] Dr. C. Kim, Prof. Dr. T. Fujigaya, Prof. Dr. N. Nakashima
Department of Applied Chemistry
Kyushu University, 744 Moto-oka
Nishi-ku, Fukuoka 819-0395 (Japan)
E-mail: fujigaya-tcm@kyushu-u.ac.jp
nakashima-tcm@kyushu-u.ac.jp

Supporting Information and the ORCID identification number(s) for the author(s) of this article can be found under: https://doi.org/10.1002/cphc.201700815.

An invited contribution to a Special Issue on CO_2 Utilisation

by tuning the electrolyte composition (cation, anion, pH, concentration),[8] we can achieve a partial current density for CO as high as 440 mA cm^{-2} at energy efficiencies of ≈42%, for the case of using Ag nanoparticles coated GDE as the cathode with an IrO_2 anode and 3.0 M KOH electrolyte. In other work, Dufek et al. have reported a system operating at elevated temperature and/or pressure that produces current densities as high as 350 mA cm^{-2} in combination with a Faradaic efficiency of 82% for CO, specifically, but at an energetic efficiency of less than 30%.[9] This low energy efficiency is insufficient for an economically viable process, which probably would require an energy efficiency of >60%.[10] Currently no catalysts or electrochemical systems are known that exhibit sufficient activity (i.e., >150 mA cm^{-2}) at a sufficiently low cathode overpotential (< 0.5 V) to ensure high energy efficiencies. Prior experimental and computational studies suggest that Au might be a better catalyst than the frequently studied Ag.[4,6c,11] For example, Au nanoparticles have been shown to exhibit a higher activity and a lower onset for the electroreduction of CO_2 to CO than Ag.[6c] However, Au nanoparticles are known to lack stability due to aggregation.[6c]

A common approach to lower the loading of precious metal catalyst is the use of high-surface-area catalyst supports such as carbon black, titanium dioxide, or carbon nanotubes (CNTs).[12] This approach may also improve catalyst stability (e.g., by preventing particle aggregation). Among these various catalyst supports, CNTs provide high electrical conductivity, good electrochemical durability, and high surface area to support catalyst particles. Catalyst nanoparticles can be deposited on CNTs using a variety of deposition methods including impregnation, ultrasound, sputter deposition, precipitation, and electrochemical deposition.[12] To overcome their chemically inert nature, CNTs are often oxidized using a strong acid solution (mixture of H_2SO_4 and HNO_3) to introduce COOH and OH groups on the surface to make the surface more hydrophilic, thus enhancing the binding of metal nanoparticles to CNTs.[12,13] However, treatment with strong acid also affects the durability of CNT-based electrocatalysts.[13] An alternative approach to enhance nanoparticle adhesion that does not involve oxidation with strong acid involves wrapping multi-wall carbon nanotubes (MWNTs) with thin (<1 nm) polymeric layers of polybenzimidazole (PBI) and pyridine-containing polybenzimidazole (PyPBI) that can provide nucleation sites for the in situ growth of metal nanoparticles.[13,14] Although the polymers by themselves are not electronically conductive, the sub 1 nm thickness ensures an electronic contact between the MWNTs and metal nanoparticles via quantum tunneling.[15] In prior work, some of us have used the resulting polymer-wrapped MWNTs, on which Pt nanoparticles were deposited, as catalyst for the oxygen reduction reaction (ORR) in both acidic and alkaline fuel cells.[13,14] Compared to Pt on carbon black or Pt on oxidized MWNTs, the highly-dispersed Pt nanoparticles (particle size: 3.2±0.78 nm) on the polymer-wrapped MWNTs exhibit increased catalyst activity as a result of a higher electrochemically active surface area (ECSA) while still providing high catalyst stability at low Pt loadings (0.45 mg cm^{-2}).

Here, we adopt this strategy to obtain a highly active and stable catalyst for CO_2 reduction: Au nanoparticles supported on polymer wrapped MWNTs (MWNT/PyPBI/Au, Figure 1). We expect that this approach 1) will ensure a low loading of Au; 2) will yield surface-bound Au nanoparticles in a size range that provides a high electrochemically active surface area and thus high activity; and 3) will prevent Au-nanoparticle aggregation, which is typically observed when they are supported via other methods. For comparison, we also created a similar catalyst supported on polymer-wrapped carbon black (CB/PyPBI/Au) and compared its performance in the electroreduction of CO_2 to the performance of the MWNT/PyPBI/Au catalyst.

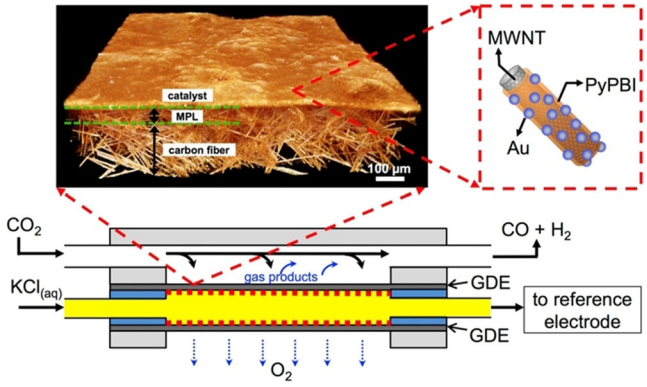

Figure 1. Top-right: Schematic representation of the Au catalyst supported on polymer-wrapped multiwall nanotubes (MWNT/PyPBI/Au) studied here. This catalyst is deposited on a gas diffusion electrode (Top-left; Reconstructed 3D view obtained from MicroCT data) at a loading of 0.17 mg Au cm^{-2}. Bottom: Schematic representation of the microfluidic electrolysis cell used in this study for the electroreduction of CO_2 to CO. The anode is comprised of Pt deposited on a second gas diffusion electrode.

2. Results and Discussion

2.1. Catalyst Synthesis and Characterization

The synthesis procedures of the MWNT/PyPBI/Au and CB/PyPBI/Au catalysts as well as the corresponding TEM images are shown in Figure 2. First, the MWNT/PyPBI (or CB/PyPBI) catalyst support was prepared by suspending the MWNTs (or CB) in a solution of PyPBI in *N*,*N*-dimethylacetamide (DMAc). The mixture was sonicated for 4 h to ensure uniform wrapping with the PyPBI. The mixture was then filtered, rinsed, and dried under vacuum to yield either the MWNT/PyPBI or the CB/PyPBI catalyst support. Second, Au nanoparticles were grown in situ on the surfaces of these two catalyst supports. Specifically, the MWNT/PyPBI (or CB/PyPBI) powder was re-suspended in an ethylene glycol/water mixture ($^{v}/_{v}$=3/2). Chloroauric acid ($HAuCl_4$) was dissolved in the same solvent mixture. Then, the two solutions were mixed in a certain ratio, and upon the addition of sodium borohydride ($NaBH_4$) reduction of Au^{III} to Au^0 was induced, leading to nanoparticle nucleation and growth of Au particles on the MWNT/PyPBI (or CB/PyPBI) support. The two products were obtained after extensive stirring and filtration. Further details are provided in the Experimental Section and in the Supporting Information (SI).

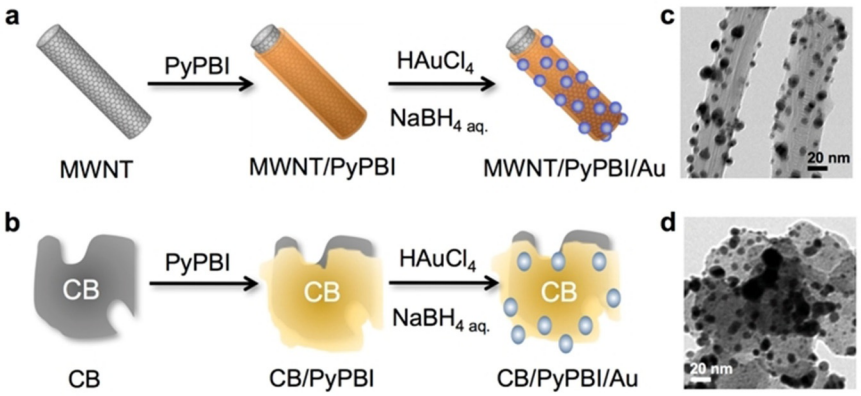

Figure 2. Synthesis procedure of the as-produced catalysts. Schematic representation of the preparation of: a) MWNT/PyPBI/Au and b) CB/PyPBI/Au used in this study. TEM images of the as-synthesized catalysts: c) MWNT/PyPBI/Au (50 wt.% Au) and d) CB/PyPBI/Au catalyst (45 wt.% Au).

We characterized the MWNT/PyPBI/Au and CB/PyPBI/Au catalysts using TEM (Figure 2c,d), XRD (Supplementary information Figure S1) and thermal gravimetric analysis (TGA). Figure 2c and 2d show that 1–20 nm-Au nanoparticles are uniformly embedded on the surfaces of the MWNT/PyPBI and CB/PyPBI supports. The XRD diffraction patterns show that the Au nanoparticles in all Au-based samples are polycrystalline. The TGA measurements show that the Au content of the MWNT/PyPBI/Au and CB/PyPBI/Au samples is 50 and 45 wt.%, respectively.

2.2. Electrochemical Characterization

Electrochemical characterization revealed that the MWNT/PyPBI/Au outperformed the CB/PyPBI/Au as well as unsupported Au, and Au supported on carbon black (CB/Au) for the reduction of CO_2 to CO (Figure 3). We performed these tests in a previously reported microfluidic CO_2 electrolysis cell (Figure 1),[16] using gas diffusion electrodes (GDEs) that were covered with the different catalysts, all at identical metal loading (0.17 mg Au cm^{-2}), and deposited using an automated airbrush method.[17] The results in Figure 3 show that under ambient conditions the different Au-based catalysts yield different partial current densities for CO production. The lowest current densities for CO are found with the Au particles deposited directly onto the GDE surfaces. Increasingly higher partial current densities for CO are achieved for the Au-based catalysts supported on CB (CB/Au), supported on polymer-wrapped CB (CB/PyPBI/Au), and supported on polymer-wrapped MWNT (MWNT/PyPBI/Au). The polymer wrapping (PyPBI) by itself was found not to significantly affect the selectivity of CO_2 electroreduction, as is evident from the FE_{CO} data for CB/PyPBI/Au and

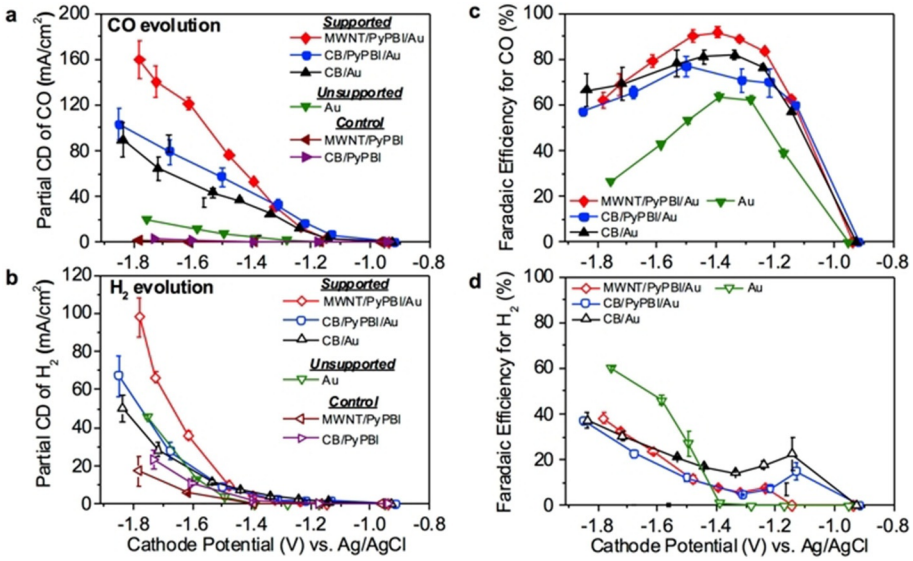

Figure 3. Results of electrochemical reduction of CO_2 in a flow reactor. Partial current density of: a) CO and b) H_2 as well as Faradaic efficiency for c) CO and d) H_2 as a function of cathode potential (V) vs. Ag/AgCl. The error bars represent the standard deviation of the average of three experiments ($N=3$). Cathode catalyst: 0.34 mg cm^{-2} MWNT/PyPBI/Au (50 wt% Au, ca. 0.17 mg Au cm^{-2}); 0.38 mg cm^{-2} CB/PyPBI/Au (45 wt% Au, ca. 0.17 mg Au cm^{-2}); 0.28 mg cm^{-2} CB/Au (60 wt% Au, ca. 0.17 mg Au cm^{-2}); 0.16 mg cm^{-2} Au; 0.19 mg cm^{-2} MWNT/PyPBI; 0.19 mg cm^{-2} CB/PyPBI. Anode catalyst: 4.25 mg cm^{-2} Pt black. Reactant streams: 7 sccm CO_2. Electrolyte: 1.0 M KCl flowing at 0.5 mL min^{-1}. Data collected at room temperature and ambient pressure.

CB/Au (Figure 3c). The MWNT/PyPBI/Au catalyst shows a partial current density of 160 mA cm^{-2} for CO production at a potential of −1.78 V vs. Ag/AgCl under ambient conditions (Figure 3a). In comparison, the CB/PyPBI/Au and CB/Au reach a partial current density for CO of 90–100 mA cm^{-2} at similar cathode potentials, while all other catalysts and control samples exhibited significantly lower current densities.

We also characterized the different catalysts using a conventional three-electrode electrochemical cell, specifically to determine their electrochemically active (exposed) surface areas (ECSAs) by comparing the area of the cathodic Au oxide stripping peak observed for each sample (SI, Figure S2).[18] The results obtained by these measurements, summarized in Table 1,

Table 1. Summary of results obtained from cyclic voltammetry of samples with Au content. Estimation of Au electroactive surface area using charge associated with stripping of the Au surface oxide (420 μC cm^{-2})[19] and electrical charge associated with the integration of the oxide peak between the potential limits of 0.9 to 0.5 V.[18,20] Three independent trials, each with recast electrodes, are factored into each average value reported.

Catalyst	Electrical charge [μC]	Specific electrochemically active surface area [m^2/g Au]
Au	110 ± 40	3 ± 1
CB/Au	410 ± 80	10 ± 2
CB/PyPBI/Au	740 ± 100	18 ± 3
MWNT/PyPBI/Au	950 ± 50	23 ± 1

demonstrate that the MWNT/PyPBI/Au catalyst exhibits the highest ECSA (23 m^2 g^{-1} Au), about 25% higher than the ECSA obtained for the CB/PyPBI/Au catalyst, at least twice as high as the ECSA obtained for the CB/Au catalyst, and ≈8 times higher than the ECSA obtained for unsupported Au particles (unsupported Au < CB/Au < CB/PyPBI/Au < MWNT/PyPBI/Au). These increases in ECSA for the different catalysts correspond qualitatively with the trends in the observed relative partial current densities for CO. This suggests that the catalytic performance enhancements observed can be attributed largely to the increase in ECSA when the catalytically active nanoparticles are deposited in an unsupported fashion or on different support materials.

We also measured the reduction activity of the different catalysts and of the support materials without Au using a conventional three-electrode electrochemical cell in the presence of CO_2 or Argon feed (SI, Figure S3). The polymer-wrapped supports (MWNT/PyPBI and CB/PyPBI) exhibit identical performance in Ar and CO_2, suggesting that they are unable to reduce CO_2 (Figure S3a,b). In contrast, the MWNT/PyPBI/Au catalyst exhibits a significantly larger reduction current in the presence of CO_2 than in Ar, presumably due to its high ECSA and its selectivity to form CO (Figure S3c–f).

Figures 3c and 3d show the Faradaic efficiencies for CO and H_2 for the various catalyst samples and controls deposited on the gas diffusion electrodes that were tested in the microfluidic flow cell. At cathode potentials up to −1.5 V (vs. Ag/AgCl), the catalysts exhibit a selectivity similar to what has been observed previously for unsupported Au. After the onset region (at approximately −1.0 to −1.1 V), the Faradaic efficiency for CO rapidly climbs to stable levels of 80–100%. The electrodes with MWNT/PyPBI/Au as the catalyst exhibit the best selectivity for CO, exceeding 90%. At cathode potentials exceeding −1.5 V, a drop in the selectivity for CO is apparent for all Au-based samples. In part, this can be explained by the increased evolution of H_2, whose production is known to be catalyzed by carbon supports at these potentials.[17] Also, large amounts of gaseous CO and H_2 are produced at these cathode potentials leading to the formation of bubbles in the flow cell, possibly lowering the amount of reaction products that is recorded in the GC analysis of the product mixture.

Next, we also tested the stability of the MWNT/PyPBI/Au catalyst. The experiments were performed in a three-electrode cell instead of a flow cell to eliminate degradation effects due to the GDL. For these stability experiments, the cell potential was held constant at −1.6 V over 26 h. During this time, the catalyst slowly improved in performance by about 12% (SI, Figure S4). A change in performance for a freshly prepared electrode such as those used here is not unusual; for example fuel cell electrodes are known to need a certain break-in period before their performance levels off.[21]

3. Conclusions

In conclusion, the results reported here demonstrate that MWNT/PyPBI has promise as a catalyst support for Au nanoparticles: The Au particles grown are small (1–20 nm), well dispersed, and they perform well in the electrochemical reduction of CO_2 to CO. The maximum current density of 160 mA cm^{-2} exceeds the performance levels obtained when using CB/PyPBI/Au, unsupported Au, or Au supported on carbon black (CB/Au) catalysts. Furthermore, use of the MWNT/PyPBI support seems to prevent degradation or aggregation of the Au particles, resulting in stable electrocatalytic performance. Although, high levels of CO activity were obtained at low Au loadings (0.17 mg cm^{-2}), future work could focus on a further investigation of the effect of loading on catalyst utilization, with the aim of providing more fundamental insights (kinetic vs. mass transfer limitations, structural effects) into electrode design. Furthermore, now that several active, selective, and stable catalysts for CO_2 electroreduction (such as the MWNT/PyPBI/Au reported here) are available in the literature, future work should focus on understanding the factors (ion migration, local pH, change in hydrophobicity, etc.) affecting the stability/durability of catalyst and GDE at industrially relevant current densities (> 100 mA cm^{-2}).

From a more general perspective, the approach of wrapping MWNTs with a polymer to obtain a catalyst support material that stabilizes highly active precious metal catalyst particles may also be beneficial for other electrocatalysis applications, for example the reduction of CO_2 to products other than CO using catalysts other than Au. Moreover, the polymer-wrapped MWNT-supported Au catalyst reported here may be promising

for other catalytic reactions known to be catalyzed by Au, for example for low-temperature water gas shift reactions and NO reduction with hydrocarbons, which are both of industrial relevance.

Experimental Section

Preparation of the MWNT/PyPBI/Au Catalyst

The pyridine-containing polybenzimidazole (poly[2,2′-(pyridine- 2,6-diyl)bibenzimidazole-5,5′-diyl]), PyPBI, was prepared using the previously described method.[14a] To wrap the MWNTs (Nikkiso Co., Ltd.) with PyPBI, 4 mg of PyPBI was dissolved in 20 mL of *N*,*N*-dimethylacetamide (DMAc), followed by addition of 20 mg of the MWNTs. The resulting mixture of the MWNTs and PyPBI in DMAc was then sonicated for 4 h to ensure uniform wrapping of the MWNTs with the PyPBI. After sonication, the mixture was filtered using PTFE filter paper (0.2 μm pore size, Millipore) and rinsed with DMAc twice to remove residual PyPBI, followed by drying overnight under vacuum. The resulting black powder is herein referred to as MWNT/PyPBI.

The synthesis of Au NPs on the MWNT/PyPBI is performed as follows. First, 5 mg of MWNT/PyPBI powder was dispersed in a 10 mL ethylene glycol/water mixture (*v*/*v* = 6/4) via sonication for 1 h. Second, aq.1.4 mM $HAuCl_4$ (4.5 mg Au, Wako Pure Chemical Industries, Ltd.) was diluted with 15 mL of an ethylene glycol/water mixture (*v*/*v* = 4/1). Next, the MWNT/PyPBI suspension was added into the dilute $HAuCl_4$ solution to which, after stirring for 5 min, 3 mL of 0.1 mM $NaBH_4$ in water was added. The mixture of MWNT/PyPBI, $HAuCl_4$ and $NaBH_4$, ethylene glycol and water was continually stirred for 24 h at room temperature under N_2. The mixture was then filtered using a PTFE filter paper (0.1 μm pore size, Millipore) and dried overnight under vacuum. The resulting black powder is herein referred to as MWNT/PyPBI/Au. The MWNT/PyPBI/Au consists of 50 wt.% Au and 50 wt.% MWNT/PyPBI as measured using the thermal gravimetric analysis (TGA).

Three-Electrode Cell Operation

High purity water (18 MΩ) was obtained from a Millipore water purification system. All reagents were analytical grade and used as received. The three-electrode cell experiments were carried out using a CH Instruments bipotentiostat. The two-compartment electrochemical cell consisted of a Au wire counter electrode, isolated from the working electrode via a frit, and a "no-leak" Ag/AgCl reference electrode (Cypress), separated from the working electrode by means of a Luggin capillary. Electrochemical measurements were all recorded and reported versus the Ag/AgCl electrode. The catalysts for the three electrode cell experiments were prepared as follows. Catalyst inks containing the powder catalyst (enough to contain 1.0 mg Au) and Nafion (5 wt%, Aldrich) in a mass ratio of catalyst to Nafion of 30/1 were prepared in 1 mL of an isopropyl alcohol/H_2O mixture (v/v = 4/1) and sonicated prior to electrode preparation. A 10 μL drop of the catalyst ink was deposited and dried under flowing Ar on a rotating ring-disk electrode (Pine Instruments), comprised of a polished (0.05-micron alumina) glassy carbon disk electrode (0.196 cm^2) with a Pt ring.

Prior to measurements of reduction activity as well as the ECSA measurements, the electrochemical cell was purged with Ar gas. Gas flow was then redirected to maintain Ar flow over the top of the 1 M KCl (≥99.9995% Sigma Aldrich) or 0.5 M H_2SO_4 (J. T. Baker) electrolyte solution. Data collection under CO_2 first involved purging the electrolyte solution, followed by the reduction of gas flow into the electrolyte solution prior to data collection.

Electrochemical Measurements in a Flow Cell

Preparation of Electrodes: The gas diffusion electrodes were prepared by depositing the catalyst ink onto the Sigracet 35 BC gas diffusion layers (GDL, Ion Power) via an air-brush method for the cathode and hand painting for the anode.[17] The preparation of catalyst inks for cathodes is as follows:

1) Au catalysts (MWNT/PyPBI/Au, CB/PyPBI/Au, CB/Au, Au): Catalyst inks containing the powder catalyst (enough to contain 0.17 mg cm^{-2} Au) and Nafion (5 wt.% Nafion solution, Aldrich) in a mass ratio of catalyst to Nation of 30/1 were prepared in 1 mL of an isopropyl alcohol/H_2O mixture (*v*/*v* = 4/1) as the carrier solvents.

2) Control samples (MWNT/PyPBI, CB/PyPBI): Catalyst inks containing the polymer-wrapped supports (enough to contain 0.19 mg cm^{-2} MWNT/PyPBI or CB/PyPBI) and Nafion (5wt.% Nafion solution, Aldrich) in a mass ratio of catalyst to Nation of 30/1 were prepared in 1 mL of an isopropyl alcohol/H_2O mixture (*v*/*v* = 4/1) as the carrier solvents.

For the hand-painted anodes, catalyst inks were prepared by mixing 10 mg Pt black (Alfa Aesar) and 6.9 μL Nafion solution, and adding 400 μL of Millipore water and 400 μL isopropyl alcohol as the carrier solvents. The same anode that was used for all measurements had a catalyst loading of 4.25 mg cm^{-2} Pt black. All inks were sonicated for 30 minutes to ensure uniform mixing and were either hand-painted using a paintbrush or air-brushed using an automated air-brushing deposition setup onto the teflonized carbon side of the GDL to create a GDE covered with catalyst over a geometric area of 2 cm^2. Importantly, the actual catalyst loading of the GDEs (to account for losses during the deposition) was determined by weighing the GDE before and after deposition and was indicated in all Figure captions in the paper.

Cell Assembly: Two catalyst-coated GDEs, an anode and a cathode, were placed on opposite sides of a 0.15-cm thick poly(methyl methacrylate) (PMMA) sheet with 0.5-cm wide by 2.0-cm long window (1 cm^2) such that the catalyst layers faced the flowing liquid electrolyte. The geometric surface area used to calculate current density is 1 cm^2. This three-layer assembly was clamped between two aluminum current collectors with access windows. On the cathode side, an aluminum gas flow chamber supplied CO_2, while the anode was open to the atmosphere so formed O_2 can escape. The assembly was held together with four bolts with Teflon washers to maintain electric isolation between the electrodes.

Electrochemical Testing Procedures: CO_2 electrolysis experiments were conducted using a potentiostat (Autolab PG30) at room temperature and ambient pressure. CO_2 gas (S.J. Smith, 100%) was fed at a rate of 7 sccm. In all experiments, the electrolyte flow rate was 0.5 mL min^{-1} controlled by a syringe pump (Harvard Apparatus, PhD 2000). The electrolyte was 1 M KCl (Sigma–Aldrich, ≥99.9995% pure) in water. Millipore water was used for all electrolytes. Electrolysis cell polarization curves were obtained by steady-state chronoamperometric measurements at different potentials, in which gaseous products, as well as unreacted CO_2, were collected and injected into an on-line gas chromatograph (Trace GC, ThermoFisher Scientific) equipped with a thermal conductivity detector for quantitative determination of product composition. Specifically, for the chronoamperometric measurements, the current was allowed to stabilize for 180 s after stepping onto a potential and before the

gas analysis was performed. Gas samples were analyzed using a triple injection method i.e., three gas injections were made at regular intervals over a 180 s time period and the average peak area was used for quantification. The current was also averaged over the 180 s time period to account for fluctuations due to bubble formation. Individual anode and cathode polarization curves were independently measured using an external Ag/AgCl reference electrode which was ionically connected to the electrolyzer. All the potentials reported in this work represent actual readings and were not *iR* corrected. The Faradaic efficiency and partial current density calculations were performed according to the procedure described earlier.[17]

Acknowledgements

We gratefully acknowledge financial support from the Department of Energy (DE-FG02005ER46260), the Department of Energy through an STTR grant to Dioxide Materials and UIUC (DE-SC0004453), the National Science Foundation (CTS 05-47617), and the International Institute for Carbon Neutral Energy Research (WPI-I2CNER), sponsored by the Japanese Ministry of Education, Culture, Sports, Science and Technology.

Conflict of interest

The authors declare no conflict of interest.

Keywords: Au nanoparticles · carbon nanotubes · catalysts · CO_2 reduction · electrodes

[1] S. J. Davis, K. Caldeira, H. D. Matthews, *Science* **2010**, *329*, 1330 – 1333.
[2] a) S. Pacala, R. Socolow, *Science* **2004**, *305*, 968 – 972; b) S. J. Davis, L. Cao, K. Caldeira, M. I. Hoffert, *Environ. Res. Lett.* **2013**, *8*, 011001.
[3] a) H. R. M. Jhong, S. Ma, P. J. A. Kenis, *Curr. Opin. Chem. Eng.* **2013**, *2*, 191 – 199; b) A. M. Appel, J. E. Bercaw, A. B. Bocarsly, H. Dobbek, D. L. DuBois, M. Dupuis, J. G. Ferry, E. Fujita, R. Hille, P. J. A. Kenis, C. A. Kerfeld, R. H. Morris, C. H. F. Peden, A. R. Portis, S. W. Ragsdale, T. B. Rauchfuss, J. N. H. Reek, L. C. Seefeldt, R. K. Thauer, G. L. Waldrop, *Chem. Rev.* **2013**, *113*, 6621 – 6658; c) D. T. Whipple, P. J. A. Kenis, *J. Phys. Chem. Lett.* **2010**, *1*, 3451 – 3458.
[4] Y. Hori, H. Wakebe, T. Tsukamoto, O. Koga, *Electrochim. Acta* **1994**, *39*, 1833 – 1839.
[5] a) M. E. Dry, *Catal. Today* **2002**, *71*, 227 – 241; b) D. Leckel, *Energy Fuels* **2009**, *23*, 2342 – 2358.
[6] a) A. J. Martín, G. O. Larrazabal, J. Perez-Ramirez, *Green Chem.* **2015**, *17*, 5114 – 5130; b) B. Kumar, J. P. Brian, V. Atla, S. Kumari, K. A. Bertram, R. T. White, J. M. Spurgeon, *Catal. Today* **2016**, *270*, 19 – 30; c) Y. H. Chen, C. W. Li, M. W. Kanan, *J. Am. Chem. Soc.* **2012**, *134*, 19969 – 19972; d) W. L. Zhu, R. Michalsky, O. Metin, H. F. Lv, S. J. Guo, C. J. Wright, X. L. Sun, A. A. Peterson, S. H. Sun, *J. Am. Chem. Soc.* **2013**, *135*, 16833 – 16836; e) H. Mistry, R. Reske, Z. H. Zeng, Z. J. Zhao, J. Greeley, P. Strasser, B. R. Cuenya, *J. Am. Chem. Soc.* **2014**, *136*, 16473 – 16476; f) Y. Yoon, A. S. Hall, Y. Surendranath, *Angew. Chem. Int. Ed.* **2016**, *55*, 15282 – 15286; *Angew. Chem.* **2016**, *128*, 15508 – 15512; g) Q. Lu, J. Rosen, Y. Zhou, G. S. Hutchings, Y. C. Kimmel, J. G. G. Chen, F. Jiao, *Nat. Commun.* **2014**, *5*, 3242.
[7] S. Ma, R. Luo, S. Moniri, Y. Lan, P. J. A. Kenis, *J. Electrochem. Soc.* **2014**, *161*, F1124 – F1131.
[8] a) M. R. Thorson, K. I. Siil, P. J. A. Kenis, *J. Electrochem. Soc.* **2013**, *160*, F69 – F74; b) B. Kim, S. Ma, H. R. M. Jhong, P. J. A. Kenis, *Electrochim. Acta* **2015**, *166*, 271 – 276; c) S. Verma, X. Lu, S. Ma, R. I. Masel, P. J. A. Kenis, *Phys. Chem. Chem. Phys.* **2016**, *18*, 7075 – 7084.
[9] a) E. J. Dufek, T. E. Lister, M. E. McIlwain, *J. Appl. Electrochem.* **2011**, *41*, 623 – 631; b) E. J. Dufek, T. E. Lister, S. G. Stone, M. E. McIlwain, *J. Electrochem. Soc.* **2012**, *159*, F514 – F517.
[10] a) M. Carmo, D. L. Fritz, J. Merge, D. Stolten, *Int. J. Hydrogen Energy* **2013**, *38*, 4901 – 4934; b) S. Verma, B. Kim, H. R. M. Jhong, S. Ma, P. J. A. Kenis, *ChemSusChem* **2016**, *9*, 1972 – 1979; c) X. P. Li, P. Anderson, H. R. M. Jhong, M. Paster, J. F. Stubbins, P. J. A. Kenis, *Energy Fuels* **2016**, *30*, 5980 – 5989.
[11] A. A. Peterson, J. K. Norskov, *J. Phys. Chem. Lett.* **2012**, *3*, 251 – 258.
[12] S. Sharma, B. G. Pollet, *J. Power Sources* **2012**, *208*, 96 – 119.
[13] T. Fujigaya, N. Nakashima, *Adv. Mater.* **2013**, *25*, 1666 – 1681.
[14] a) T. Fujigaya, M. Okamoto, N. Nakashima, *Carbon* **2009**, *47*, 3227 – 3232; b) M. Okamoto, T. Fujigaya, N. Nakashima, *Small* **2009**, *5*, 735 – 740; c) K. Matsumoto, T. Fujigaya, K. Sasaki, N. Nakashima, *J. Mater. Chem.* **2011**, *21*, 1187 – 1190.
[15] J. Zuloaga, E. Prodan, P. Nordlander, *Nano Lett.* **2009**, *9*, 887 – 891.
[16] D. T. Whipple, E. C. Finke, P. J. A. Kenis, *Electrochem. Solid-State Lett.* **2010**, *13*, B109 – B111.
[17] H. R. M. Jhong, F. R. Brushett, P. J. A. Kenis, *Adv. Energy Mater.* **2013**, *3*, 589 – 599.
[18] S. Trasatti, O. A. Petrii, *Pure Appl. Chem.* **1991**, *63*, 711 – 734.
[19] S. Papadimitriou, A. Tegou, E. Pavlidou, S. Armyanov, E. Valova, G. Kokkinidis, S. Sotiropoulos, *Electrochim. Acta* **2008**, *53*, 6559 – 6567.
[20] I. S. Park, K. S. Lee, D. S. Jung, H. Y. Park, Y. E. Sung, *Electrochim. Acta* **2007**, *52*, 5599 – 5605.
[21] S. Srinivasan, *Fuel Cells: From Fundamentals to Applications*, Springer, Berlin, **2006**.

Manuscript received: July 20, 2017
Version of record online: October 17, 2017